Discovery of Potential Prolyl-tRNA Synthetase Allosteric Inhibitor Through Virtual Screening and *In Vitro* Assay against *Plasmodium falciparum*

Tegar Achsendo Yuniarta[1*], I Gede Ari Sumartha[1], Taufik Muhammad Fakih[2], Rosita Handayani[3], Dwi Syah Fitra Ramadhan[4]

[1] Department of Pharmaceutical Chemistry, Faculty of Pharmacy, University of Surabaya, Surabaya, Indonesia

[2] Department of Pharmacy, Faculty of Mathematics and Natural Sciences, Bandung Islamic University, Bandung, Indonesia.

[3] Department of Pharmaceutical Sciences, Faculty of Pharmacy, Airlangga University, Surabaya, Indonesia.

[4] Department of Pharmacy, Health Polytechnic of Ministry of Health, Makassar, Indonesia

ABSTRACT

Objectives: This study aimed to identify novel antimalarial compounds based on allosteric inhibitor of prolyl-tRNA synthetase using hierarchical virtual screening.

Materials and Methods: Pharmacophore model was designed initially, based on the structure-activity relationships data between several pyrazole-urea analogues and their IC_{50} enzymatic value. The model obtained was applied to screen ZINC15 database, after which followed by drug-likeness, toxicophore, and PAINS filter. The hit compounds were docked against *P. falciparum* prolyl-tRNA synthetase enzyme, using validated docking method. The resulting docking poses were ranked based on the docking score and re-evaluated based on the pharmacophore criteria. Top five compounds were obtained from this step and then evaluated using molecular dynamics simulation to verify its stability and hydrogen bond dynamics over 50 nanoseconds. MM-PBSA analysis was also performed to estimate their binding free energy. Ultimately, their potential bioactivity as antimalarial candidates have been verified against 3D7 strain.

Results: The results showed that all five compounds obtained from virtual screening possess micromolar potency *in vitro*. Two compounds (ZINC 1029449 and ZINC1029453), yield high antimalarial activity (0.44 and 0.72 μM, respectively)

Conclusions: Overall, the virtual screening approach has successfully produced lead compounds which can be further optimized to be antimalarial agents.

Keywords: Antimalarial, Molecular dynamics, *Plasmodium falciparum*, Prolyl-tRNA synthetase, Virtual screening.

1. INTRODUCTION

Malaria is a global public health concern, particularly in developing countries worldwide[1]. This infectious disease is caused by Plasmodium species, specifically P. falciparum and P. vivax. In 2020, an estimated total of 241 million cases occurred globally, resulting in a 12% mortality rate[2]. Furthermore, several reported case of drug resistances against common antimalarial agent[2] has underlined the necessity to search for alternative therapeutic candidate which is safe and more effective.

High-throughput screening is an integral part of the early drug discovery and development process, allowing the simultaneous assay of multiple compounds at a rate of up to tens of thousands of compounds per week[3]. Due to advancements in computer science and technology, this process can now be simulated in silico, significantly

reducing the time and resources spent on trial and error in the laboratory while increasing the hit probability for bioactivity screening[4]. This approach, known as virtual screening, has been widely applied with success in generating hits for various biological targets, including the identification of potential compounds with antimalarial activity[5,6]. Virtual screening encompasses various computational tools from different approaches, such as ligand-based methods (pharmacophore, similarity)[7], structure-based method (molecular docking, molecular dynamics)[8–10] or artificial intelligence-based method[11,12]. These tools can be employed subsequently or in parallel to identify the best compounds, which are then tested in vitro. Moreover, this process can be integrated with high-throughput screening to yield more potent lead compounds[4].

Aminoacyl-tRNA synthetases (aaRs) are a family of enzyme which are responsible for esterification of amino acid with cognate tRNA in two-step reaction. Firstly, amino acid will react with ATP to produce amino acid-AMP complex with pyrophosphate anion as side product. Subsequently, hydroxyl group of tRNA attack carbonyl group of amino acid-AMP complex, thus displacing AMP in the complex. The reaction ultimately yields amino acid-tRNA complex, which then delivered to ribosome to take part in protein synthesis. There are 20 aaRS enzymes, which correspond to the total of amino acid in nature[13]. This enzyme has garnered some interest recently, notably as potential druggable target in various infectious diseases

such as malaria[14]. To date, 36 aminoacyl-tRNA synthetases are known to reside inside apicoplast, mitochondria, or cytoplasm of *Plasmodium falciparum*, of which five enzymes have been structurally characterized[14]. Prolyl-tRNA synthetase (PfPRS) is one of the examples. Its significance was first known in the 2010s as the main target of febrifugine, halofuginone, and their other derivates activity [15–18]. Crystallographic data shows that febrifugine and its analogues inhibit PfPRS by occupying tRNA and L-proline binding site [16,18].

This dual site binding mechanism is observed not only in *Plasmodium falciparum* but also in human orthologue (HsPRS) [18,19], due to the very high homology between the two. Upon examination, it can be observed that PfPRS shares around 54% similarities with HsPRS. The difference lies in the zinc binding motif, which exists only in HsPRS. A slight deviation can also be found in anticodon binding domain [18]. Nevertheless, it is shown that febrifugin-like compound binds in the same manner on both orthologues, making their selectivity questionable.

Recent study showed novel binding mode of PfPRS via allosteric regulation, which yield higher selectivity against HsPRS. Based on high-throughput screening result, it was found that pyrazole-urea based compound possess selective activity towards PfPRS and promisingly potent scaffold against *Plasmodium falciparum* [20] (**Figure 1**). This allosteric ligand is in the vicinity of ATP binding site, specifically in the TXE loop. In the process, it displaces the loop from the conservative conformation [18] (**Figure 2).**
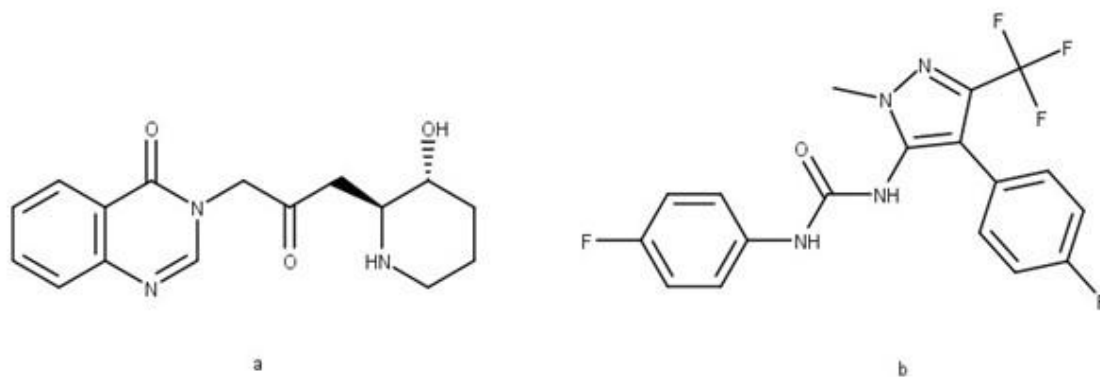
Figure 1. Chemical structure of febrifugine (a) and TCMDC-124506 (b), an orthosteric and allosteric inhibitor of PfPRs enzyme, respectively.
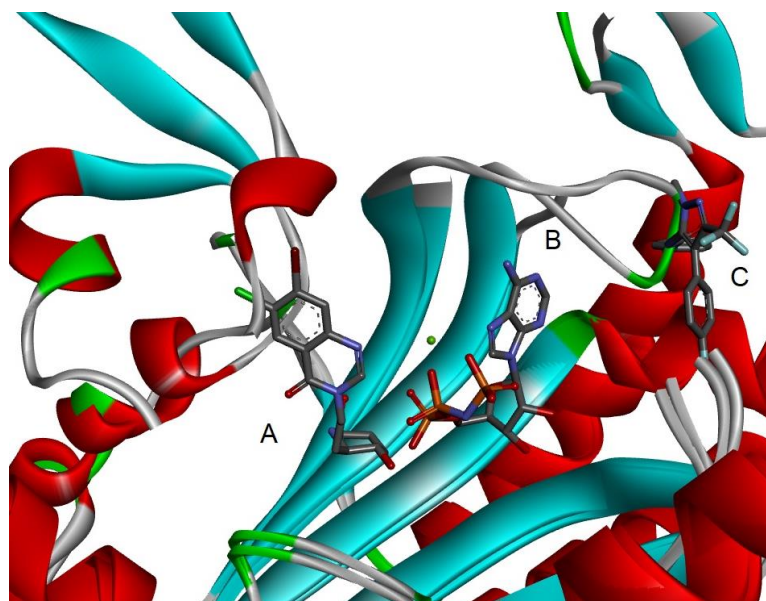
Figure 2. Overlay image of two PfPRS crystal structure containing halofuginone-AMPPNP and TCMDC-124506, respectively. (A=halofuginone; B=AMPPNP, an ATP analogue; C=TCMDC-124506)

In addition, several plant-based compounds have been predicted to possess specific enzymatic activity toward PfPRS using virtual screening and molecular dynamics[21]. In this study, a similar approach was implemented in attempt to identify potential selective PfPRS inhibitor among commercially available compounds in ZINC database[22]. Ultimately, antimalarial activity of the compounds obtained through this process were verified by *in vitro* assay against *Plasmodium falciparum* strain 3D7.

2. METHODS

2.1. Phamacophore Modelling and Screening

Pharmit webserver (https://pharmit.csb.pitt.edu/) was used for virtual screening[23]. Our protocol commenced with structure-based pharmacophore modeling using crystallographic data of PfPRS with allosteric inhibitor (**PDB ID: 4WI1**) [20]. The predetermined pharmacophore query from webserver was then modified according to known information of their structure-activity relationship[20]. Resulting pharmacophore model was then applied to screen 13,190,317 compounds from ZINC purchasable database[22]. This procedure yielded 248 hit molecules, which were proceeded to the next step.

2.2. Drug-likeness, Toxicophore, and PAINS Filtering

The obtained compounds from previous step were filtered based on Lipinski rule of five[24] to assess their drug-likeness. In addition, possessing unwanted moieties, such as toxicophores and PAINS, were targeted for exclusion. This step was performed using FAF-Drugs 4 webserver (https://mobyle.rpbs.univ-paris-diderot.fr/cgi-bin/portal.py#forms::FAF-Drugs4)[25] The aim was to ensure that the obtained compounds are drug-like, free of toxic functional groups, and potentially not possessing promiscuous bioactivity. Criteria for defining toxic and unwanted moieties are explained in [25], while for definition of PAINS substructure are according to [26]. Notably, no compounds were found to violate all the rules. Consequently, 248 molecules proceeded to the next step.

2.3. Molecular Docking

Molecular docking step was performed using the filtered compounds from previous step and the same protein from pharmacophore modelling process (PDB ID: 4WI1) [20]. Prior to performing molecular docking, ligand and protein preparation was performed to ensure both of protein ligand represent the real condition as accurate as possible. This preparatory step includes adding hydrogen atom and partial charges of Amberff14 [27] and Gasteiger [28] for protein and ligand, respectively. The whole process of protein preparation was done in Chimera 1.14 [29] while ACC2 was used to compute partial charge of all ligands [30].

The following process was validation step. This was done to ensure the reliability of the docking method. Our approach was to evaluate the best combination of docking score and placement algorithm available in Molegro 7 Trial Version (http://molexus.io/molegro-virtual-docker/) which was used as docking software. There were two procedures of validation took place in this step. Firstly, the native ligand (TCMDC-124506) of the enzyme was removed and subsequently re-docked into the enzyme (*i.e.* self-docking/re-docking). The resulting docking pose was then superimposed to the original conformation and calculated their RMSD value, which ideally should not be over 2.0 Å[31]. Afterwards, molecular docking was performed against data set of ligands which contained both known active and inactive compounds from literature [20]. The lowest docking score obtained from each ligand was sorted ascendingly and the overall ranking was evaluated based on its area under curve (AUC) value of ROC curve [32], BEDROC [33], and standardized total gain score [34]. This calculation was done in Screening Explorer webserver [35]. The docking process was conducted in 15 Å-radius spherical region centered on native ligand.

Afterwards, the selected best method was applied to dock 248 hit molecules. The result was ranked ascendingly and evaluated subsequently according to the SAR report [20]. Five of the compounds who met the criteria, in addition to possess low docking score were selected to be processed.

2.4. Molecular Dynamics and MM-PBSA Calculation

The selected compounds from molecular docking step and the native ligand (TCMDC-12506) were then simulated using Gromacs 2016.3 simulation pack [36]. Similar forcefield and partial charge (Amberff14 [27] and Gasteiger [28]) was applied in the preparatory stage, before the docked complexes were subjected to 50 ns simulation in water and counterions (Na$^+$ & Cl$^-$). TIP3P rigid water model [37] was used in this study for its computational speed and reasonable accuracy in protein-ligand simulation [38].

Long-range electrostatic force was determined by Particle Mesh Ewald [39]. Velocity rescaling thermostat [40] and Parrinello-Rahman barostat [41] were used during NVT and NPT equilibration for 500 ps, respectively. In these processes, system temperature was adjusted to 310 K, while maintaining the pressure at 1 bar. Molecular dynamics production run was performed in a 2 fs timestep for 50 ns. The stability of the system was verified by analysis of the energy, temperature, pressure, and root-mean-square deviation (RMSD).

Afterwards, MM-PBSA calculation was performed using the G_MMPBSA package integrated in the Gromacs 2016.3 software[42]. Polar desolvation energy was calculated with the Poisson-Boltzmann equation with a grid size of 0.5 Å. The dielectric constant of the solvent was set to 80, which represents water as the solvent. Non-polar contribution was determined by calculation of the solvent-accessible surface area with the solvent radii of 1.4 Å. The binding free energy of the complex was determined based on 50 snapshots taken from the beginning to the end of the molecular dynamic simulation trajectories of the complexes.

2.5. Antimalarial Bioassay

The compounds obtained from virtual screening process were purchased from MolPort (Riga, Latvia) to be tested for their antimalarial potency. Antimalarial assay was conducted against *Plasmodium falciparum* strain 3D7. Parasites were bred in human erythrocyte using Trager-Jensen method with slight modification [43,44]. Each assay compounds were dissolved in DMSO to make 10 ppm solution. This stock solution was diluted into four other concentrations (1, 0.1, 0.01, and 0.001 ppm). 500 μL aliquot of solution was mixed with the equal amount of parasite culture in a 96 well plate, then incubated for 48 h at 37°C. This process was conducted for all five different concentrations. Chloroquine diphosphate was used as positive control. In addition, negative control was also measured using parasite culture only. Plasmodium growth was evaluated in microscope using thin blood smears preparation with Giemsa stain. Inhibition percentage can be calculated using the following equation:

$$\% \, Inhibition = \frac{(100\% - A)}{B} \, x \, 100\% \quad [44].$$

Where A and B refers to the growth percentage of compounds and negative control, respectively. Ultimately, IC_{50} values were calculated by transforming the concentration-response curve using the Probit Transformed Responses regression model. The values were expressed as a mean value with standard deviation.

3. RESULTS AND DISCUSSION

Virtual screening is currently becoming one of the most powerful tools to aid drug discovery process in cost and time-efficient manner. The method combines various drug design tools into a systematic workflow which act as a filter for the chemicals in library. This will increase the probability of finding hit and eliminate likely inactive compound[4]. There are several types of virtual screening algorithm based on their level of integration, one of which is hierarchical or classical virtual screening as implemented in this study[45]. Here we applied pharmacophore modelling, molecular docking, and molecular dynamics in a sequential order to obtain the most potentially active compounds against PfPRS enzyme.
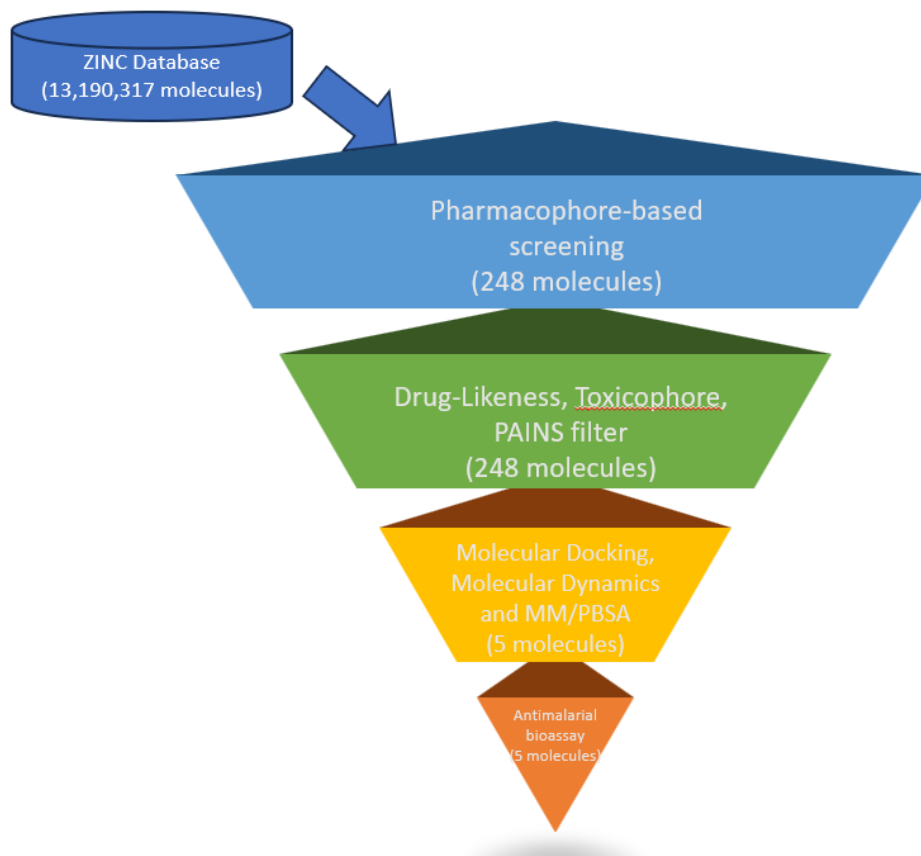
Figure 3. Workflow of virtual screening used in this study

In the beginning, pharmacophore model was built based on structure-activity relationships of pyrazole-urea analogues against PfPRS enzyme. The model was built using TCMDC-124506 as a template [20]. It consists of two aromatic ring queries on pyrazole and phenyl moiety attached to it, one hydrogen bond acceptor and two hydrogen bond donors on urea moiety, and two hydrophobic queries on N-substituent position of pyrazole and ring moiety attached to urea group. The purpose of implementing hydrophobic query instead of aromatic ring for the latter is due to the fact that glibenclamide, which contains a hydrophobic moiety, also known to possess activity against PfPRS, comparable to the TCMDC-124506 [20] (Figure 4). The resulting pharmacophore model

was then used to screen ZINC database. This process has yielded 248 molecules. All of these compounds were also passed FAF-Drugs 4 filter of toxicophore and PAINS substructure [25], ensuring the absence of potentially toxic and/or frequent-hitter compound [26].

Subsequently, molecular docking process was performed towards those compounds. Validation of this process was carried out to select the best algorithms available in Molegro 7. This docking software has three placement scorings and four docking scores. Initially, we evaluated those 12 combinations according to their RMSD value. The result showed that all but one algorithm produced docking pose with acceptable RMSD value (Figure 5).
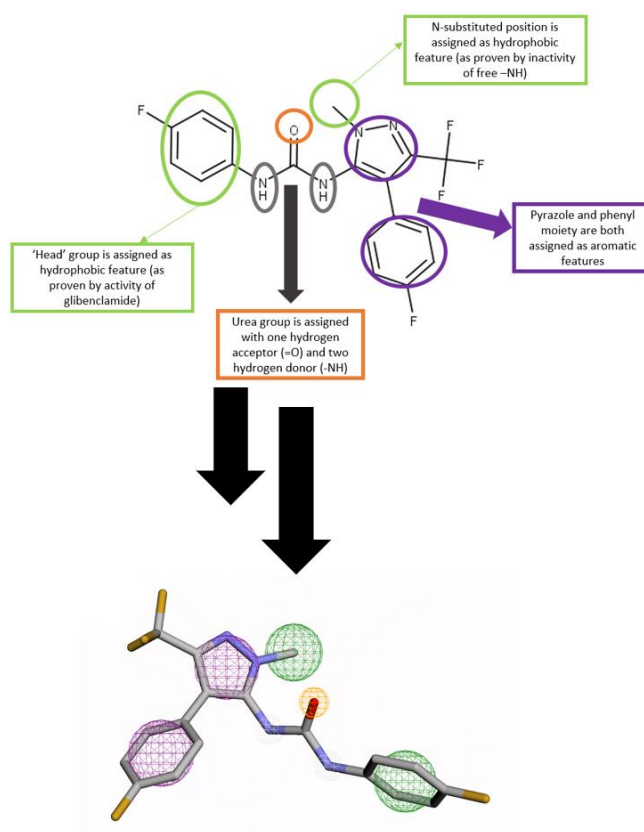
Figure 4. Pharmacophore queries of PfPRS inhibitor according to [18] (top) and its three-dimensional visualization using Pharmit webserver (bottom)

Scoring/Placement	MolDock Optimizer	MolDock SE	Iterated Simplex
MolDock Score	0.18	1.02	0.19
MolDock Score (Grid)	0.47	0.97	0.21
PLANTS Score	0.18	0.19	0.24
PLANTS Score (Grid)	3.92	0.16	0.21

RMSD Threshold ≤ 2.0 Å (RMSD value in red exceeds the threshold)

Figure 5. RMSD values calculated for 12 algorithms against PfPRS enzyme (PDB ID: 4WI1) and the superimposed ligand conformations of all the algorithm (yellow: native ligand; red: re-docking result with RMSD > 2.0 Å

The next step was to evaluate whether a method could discriminate between active and inactive compounds based on docking score-based ranking. In this context, we conducted molecular docking against analogs of pyrazole-urea whose enzymatic activity had been determined previously[20]. An alternative approach involved using putative inactive compounds, i.e., decoy compounds, as substitutes due to insufficient data on inactive compounds[46]. The evaluation was carried out based on the area under the curve values of ROC and BEDROC, as well as the Total Gain value. The ROC curve has been widely used in numerous studies as a validation tool in virtual screening campaigns[32,47,48]. This metric ranges from 0 to 1, representing the complete inability and perfect capability of a method to separate active and inactive compounds, respectively[49]. BEDROC is a modification of the ROC curve that applies Boltzmann

distribution to enhance its ability to discriminate early hits in virtual screening [31]. Meanwhile, Total Gain is a statistical tool used to quantify the score of the virtual screening process in explaining compound bioactivity. This parameter is akin to the determination coefficient, where the value ranges from 0 to 1, representing the explanatory power of the virtual screening method[34,50]. From this validation step, it was found that only one algorithm (MolDock Score-MolDock Optimizer) works best to enrich active molecule and in accord with all validation metrics (**Table 1**). MolDock Score is a docking score based on piecewise linear potential (E_{PLP}) with additional terms namely hydrogen bonds direction [51]. MolDock Optimizer is a placement algorithm based on differential evolution algorithm. This method is identical to genetic algorithm, albeit the result is more guided by addition of weighted difference of previous calculation [51].
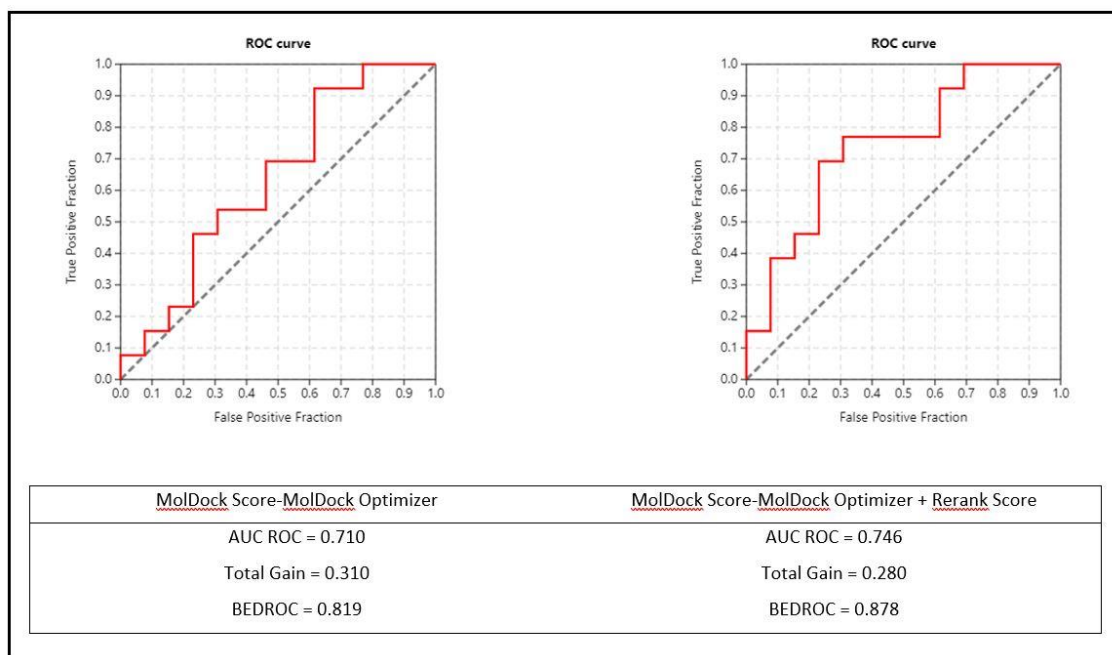
Table 1. AUC ROC, Total Gain, and BEDROC values calculated for 11 algorithms against PfPRS enzyme (PDB ID: 4WI1)

Algorithms	AUC ROC	Total Gain	BEDROC
MolDock Score- MolDock Optimizer	**0.710**	**0.310**	**0.819**
MolDock Score- MolDock SE	0.562	0.090	0.205
MolDock Score- Iterated Simplex	0.432	0.067	0.280
MolDock Score (Grid)- MolDock Optimizer	0.615	0.157	0.161
MolDock Score (Grid)- MolDock SE	0.568	0.188	0.136
MolDock Score (Grid)- Iterated Simplex	0.574	0.081	0.720
PLANTS Score- MolDock Optimizer	0.651	0.171	0.343
PLANTS Score- MolDock SE	0.568	0.170	0.150
PLANTS Score- Iterated Simplex	0.408	0.148	0.201
PLANTS Score (Grid)- MolDock SE	0.645	0.233	0.312
PLANTS Score (Grid)- Iterated Simplex	0.503	0.074	0.618
Acceptable Threshold	>0.50	>0.25	>0.50

The virtual screening output can be further enhanced by applying a consensus scoring approach[52]. In this context, we incorporated the Rerank Score in addition to the MolDock Score to increase the discriminative power between active and inactive compounds. This method falls under the category of weighted sum ranking[52], where the

existing docking score is modified by the Lennard-Jones 12-6 potential to better depict steric factors[51]. The results showed a significant improvement based on both AUC-ROC and BEDROC values (Figure 6), signifying better early recognition of active compounds[32,33].

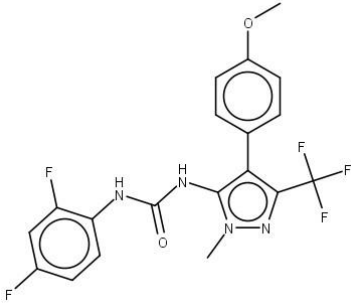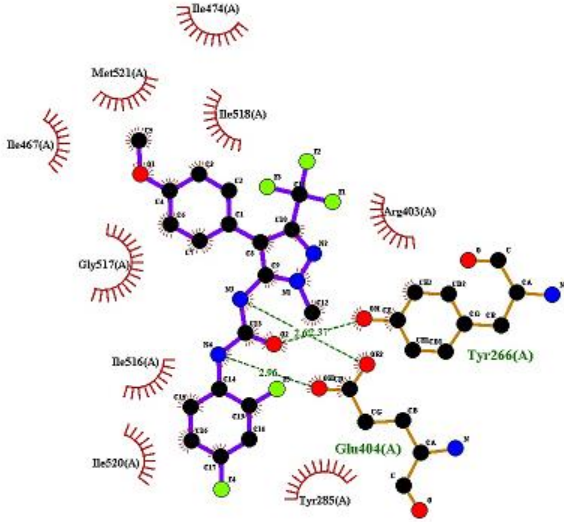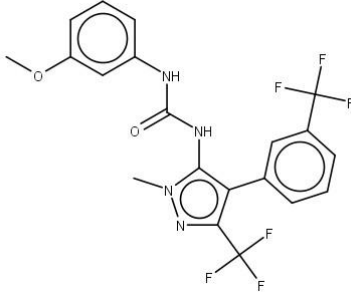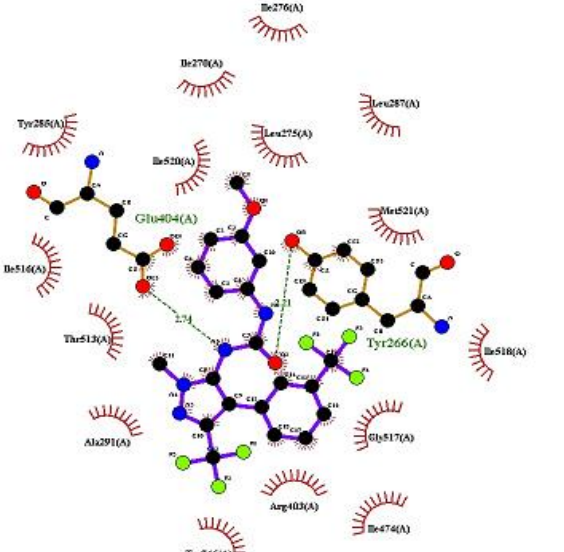| MolDock Score-MolDock Optimizer	MolDock Score-MolDock Optimizer + Rerank Score
AUC ROC = 0.710	AUC ROC = 0.746
Total Gain = 0.310	Total Gain = 0.280
BEDROC = 0.819	BEDROC = 0.878

Figure 6. Validation result of MolDock Score-MolDock Optimizer (left) and MolDock Score-MolDock Optimizer with the implementation of Rerank Score (right)

This method was then applied to dock 248 compounds obtained from pharmacophore screening. However, post-docking evaluation revealed that several high-ranked compounds possess a free NH pyrazole moiety. We decided not to select these compounds since they contradict the pharmacophore model, which specifies a N-substituted pyrazole ring. Therefore, a manual inspection was performed to choose five compounds in an ascending manner that conform to the pharmacophore model. It can be observed that most of the obtained compounds possess a pyrazole-urea moiety, with only one compound containing an isoxazole scaffold in place of pyrazole

(Table 2). Overall, the compound bearing the pyrazole-urea group ranked better than the isoxazole-urea based on their MolDock Score. These five docked compounds and TCMDC-124506 were then subjected to a 50 ns molecular dynamics simulation and MM-PBSA analysis to evaluate their conformational dynamics, structural stability, and free binding energy with the solvation model. Several parameters were evaluated post the molecular dynamics process, such as the RMSD value of the protein, RMSF plot of amino acids, and hydrogen bond occupancy of all protein complexes.

Table 2. Docking score and ligand interaction result of selected compounds

Compounds	MolDock Score +Rerank Score	Ligand Interaction*
ZINC1029449	-130.94	
ZINC1029453	-129.35	

Compounds	MolDock Score +Rerank Score	Ligand Interaction*
ZINC96133636	-126.72	

| ZINC263640015 | -121.68 | |

Compounds	MolDock Score +Rerank Score	Ligand Interaction*
ZINC3135340	-120.17	

* Ligand interaction was evaluated using LigPlot+ 2.2.4 [45] (Laskowski and Swindells, 2011).
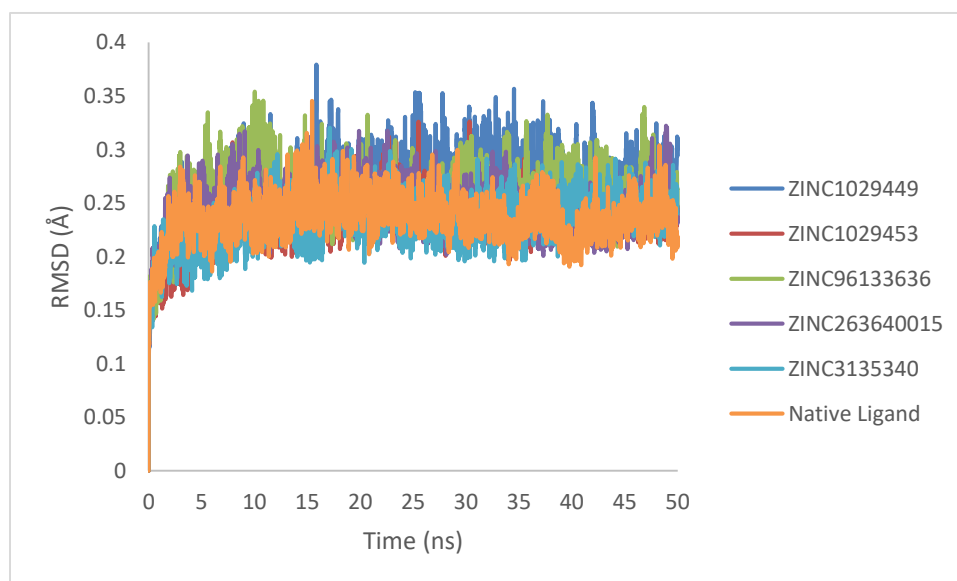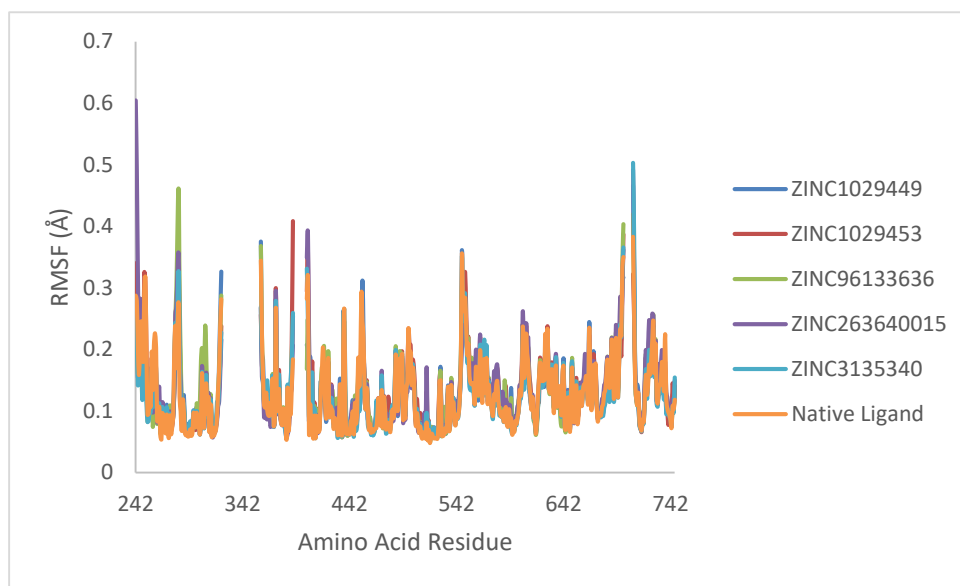
Figure 7. RMSD (above) and RMSF (below) plot of protein during 50 ns simulation

The RMSD values of the protein observed during the 10-50 ns simulation indicated the stability of all complexes. The RMSD fluctuation plot over simulation time suggested that all protein systems had reached convergence by the end of the molecular dynamics process (Figure 6). Subsequently, RMSF plots were evaluated to observe protein residue flexibility during molecular dynamics simulation. The results showed high peaks, notably in the β-hairpin structure (residue 279-283) in the catalytic domain region (CD) and the loop-α-helix structure (residue 547-554) in the anti-codon binding domain (ABD) (Figure 7).

Hydrogen bond occupancy percentage was calculated to illustrate the dynamic process of hydrogen bond interaction during the 50 ns simulation. The calculation was performed using HBonds 1.2, an integrated plugin from VMD[53]. The results, calculated as a percentage, indicate the frequency of hydrogen bond formation during molecular dynamics simulation. It was observed that, similar to the amino acid interaction in the molecular docking process, interactions with Glu404 and

Tyr266 were consistently found in almost all ligand-protein complexes. The occupancy values sometimes exceeded 100%, as seen in Glu404 interaction with ZINC102949 (116.87%). This type of interaction was also observed in the native ligand (TCMDC-124506), emerging as the only distinctive hydrogen bond interaction during the 50 ns simulation, underscoring its significance in ligand-protein interaction.

Several novel hydrogen bond interactions were also elucidated during the simulation process, such as in ZINC3135340, which formed a hydrogen bond with Thr513 and Phe405. On the other hand, it appears that two of the ligands (ZINC96133636 and ZINC263640015) showed lower values of hydrogen bond occupancy compared to the rest of the compounds, indicating a different type of ligand-amino acid interaction could take place (Table 3). Observation of the final MD snapshots also indicated several changes in ligand interaction, namely new hydrogen bond formation between ZINC3135340 and Phe405 or the absence of hydrogen bond interaction in ZINC 96133636 (Table 3). This result

generally aligns with the hydrogen bond occupancy values during the 50 ns (Table 2), where hydrogen bonds with high percentage values will be observed more frequently than the lesser ones.

Afterward, we also calculated the binding free energy of all ligands using the MM-PBSA approach. It is one of the commonly used methods to estimate ligand free energy values, aside from MM-GBSA, LIE, and alchemical binding[54–56]. This approach is an amalgamation of energy

calculation based on molecular mechanics and implicit solvent-based free energy calculation, as explained in the following equation.

$$\Delta G_{binding} = [(\Delta E_{bonded} + \Delta E_{electrostatic} + \Delta E_{van\ der\ Waals}) + (\Delta G_{polar\ solvation} + \Delta G_{surface\ area})] - T\Delta S$$

Table 3. Hydrogen bond occupancy analysis post-molecular dynamics simulation

Compounds	Hydrogen Bond Donor Occupancy*	Hydrogen Bond Acceptor Occupancy*
ZINC1029449	Tyr266 (s) (46.08%)	Glu404 (s) (116.87%)
	Phe405 (m) (0.16%)	Arg403 (m) (0.02%)
	Arg403 (s) (0.04%)	
ZINC1029453	Tyr266 (s) (57.30%)	Glu404 (s) (0.26%)
ZINC96133636	Gly283 (m) (3.22%)	Thr513 (m) (0.02%)
	Tyr285 (s) (2.38%)	Tyr285 (s) (0.02%)
	Arg403 (s) (0.32%)	
	Thr513 (s) (0.26%)	
	Phe405 (m) (0.02%)	
ZINC263640015	Tyr266 (s) (13.49%)	Glu404 (s) (3.12%)
	Tyr278 (s) (7.84%)	
	Arg514 (s) (0.02%)	
ZINC3135340	Thr513 (s) (29.93%)	Glu404 (s) (52.64%)
	Phe405 (m) (23.57%)	Tyr285 (s) (5.42%)
	Tyr266 (s) (5.76%)	Arg403 (m) (1.84%)
	Tyr285 (s) (0.16%)	
	Leu406 (m) (0.06%)	
TCMDC-124506	Tyr266 (s) (58.76%)	Glu404 (s) (63.5%)

* s = side-chain hydrogen bond; m = main hydrogen bond

The first three variables in the equation refer to molecular mechanic energy (MM), which consists of bonded and non-bonded interactions (electrostatic and van der Waals). Meanwhile, the free energy terms are made up of the total polar and non-polar contributions. In the g_mmpbsa module, these are obtained from the Poisson-Boltzmann equation (PB) and solvent-accessible surface

area (SA) value, respectively[42]. MM-PBSA approach is arguably time efficient[54] and has been implemented numerous times in virtual screening approaches to improve the reliability of protein-ligand interaction evaluation[55]. Based on the MM-PBSA calculation for 50 ns, it is observed that the compound ZINC1029449 from molecular docking possesses better binding free energy

than the rest of the compounds, including the native ligand (Table 4). We argue that hydrogen bond interaction with Glu404 plays an important role in yielding better binding free energy, followed by the Tyr266 hydrogen bond.

Ultimately, the compounds were tested for their antimalarial potency in vitro against Plasmodium falciparum chloroquine-sensitive strain (3D7). This parasite strain was chosen as it is known to express PfPRS enzyme[16,57]. According to the previous study[20], it can be expected that pyrazole-urea analogs yield antimalarial activity. The results we obtained indicate that all our assayed compounds possess micromolar inhibitory activity (Figure 8), with the top two compounds from in silico evaluation (ZINC 1029449 and ZINC1029453) being the most potent inhibitors with IC50 values of 0.44 and 0.72 μM, respectively.

**Table 4. Binding free energy of protein-ligand interaction calculated by MM-PBSA**

Compounds	$\Delta G_{binding}$	$\Delta E_{van der Waals}$	$\Delta E_{electrostatic}$	$\Delta G_{polar solvation}$	SASA
ZINC1029449	-137.146 ± 14.941	-212.072 ± 12.999	-84.083 ± 9.288	180.192 ± 16.496	-21.183 ± 0.713
ZINC1029453	-116.017 ± 15.494	-199.007 ± 15.776	-31.093 ± 13.597	135.192 ± 22.750	-21.108 ± 1.036
ZINC96133636	-102.922 ± 15.112	-209.159 ± 12.609	-5.622 ± 11.764	131.976 ± 16.185	-20.117 ± 0.868
ZINC263640015	-109.242 ± 17.206	-175.256 ± 15.315	-23.208 ± 16.997	107.706 ± 26.512	-18.483 ± 1.180
ZINC3135340	-109.879 ± 16.684	-180.185 ± 15.465	-93.073 ± 23.940	181.694 ± 24.243	-18.315 ± 1.153
TCMDC-124506	-117.262 ± 13.454	-187.746 ± 12.215	-79.158 ± 11.680	169.302 ± 17.442	-19.660 ± 0.813
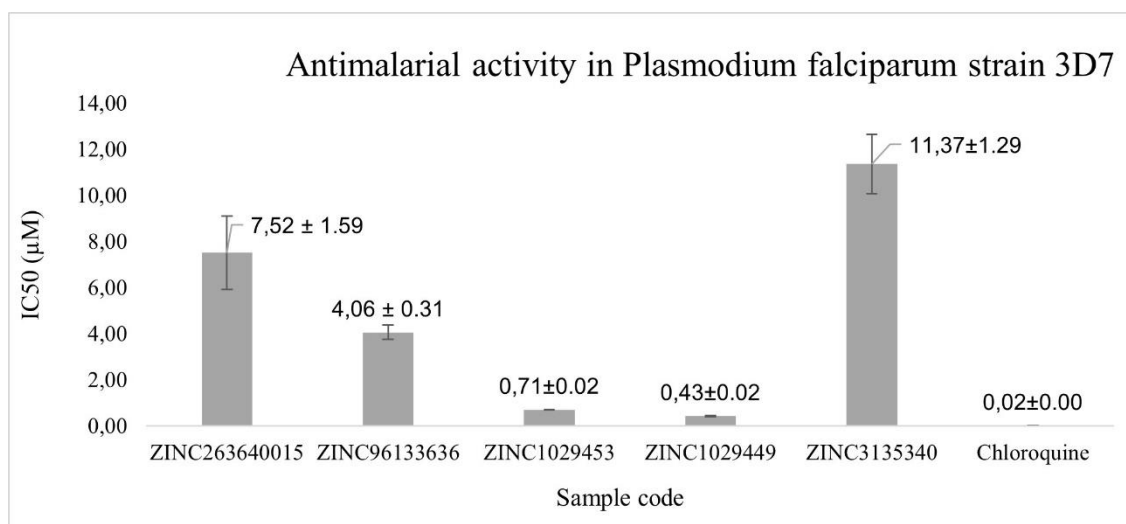
Figure 8. Antimalarial activity of five tested compounds against *Plasmodium falciparum* 3D7

All compounds bearing the pyrazole-urea scaffold perform better than the isoxazole-urea one. It is also worth noting that the in vitro assay result was generally in line with the docking score value, and the top two ranked compounds in terms of binding free energy are identical to the antimalarial assay. Compounds ZINC 1029449 and ZINC1029453 have a similar scaffold to TCMDC-124506 and its analogs, which have been tested for their antimalarial potency against both PfPRS enzyme and the 3D7 strain[20]. On the other hand, it is also found that several modifications of the 'head' and phenyl 'tail' group of the pyrazole-urea analogue slightly lower the antimalarial bioactivity. We also found that the substitution of the pyrazole moiety with the isoxazole ring has significantly reduced its potency, as shown by compound ZINC3135340 (Figure 9).
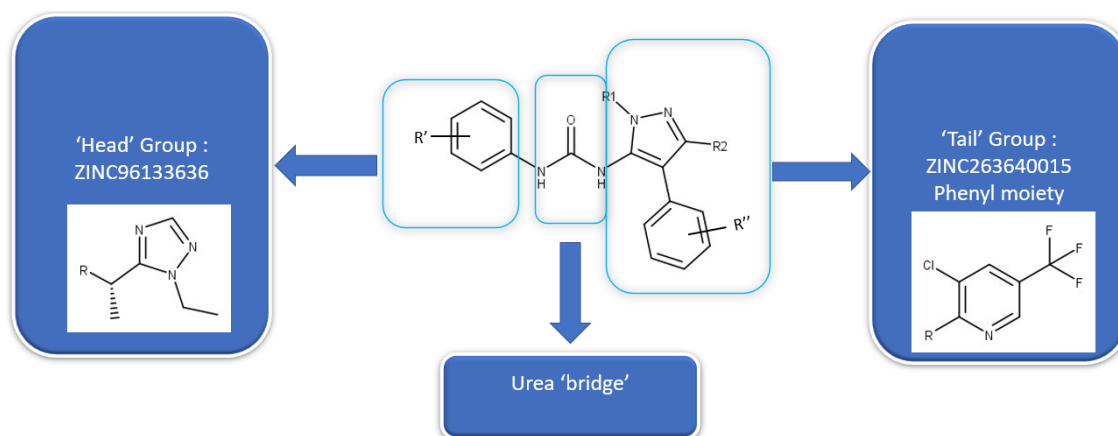
Figure 9. Common structure of pyrazole-urea based PfPRS inhbitors. Both compound ZINC96133636 and ZINC263640015 are modified at the head and tail group, respectively, from the previous SAR study [18]

4. CONCLUSION

The study conducted a hierarchical virtual screening process to identify potential antimalarial candidates through PfPRS enzyme inhibition. This method combines pharmacophore modeling, undesirable moiety filtering, molecular docking, molecular dynamics, and MM-PBSA evaluation, arranged in a sequential manner. Five compounds were discovered from this process, with four possessing a pyrazole-urea scaffold, and the fifth having an isoxazole ring in place of pyrazole. All compounds were tested for antimalarial activity against Plasmodium falciparum 3D7 and exhibited micromolar inhibitory concentrations. Two of the compounds (ZINC 1029449 and ZINC1029453) showed IC50 values of 0.44 and 0.72 μM, respectively. Further studies are still needed to verify whether the compounds inhibit the PfPRS enzyme via allosteric mechanisms.

6. CONFLICT OF INTEREST

The authors declare no conflict of interest.

REFERENCES

1. Smith RD, Keogh-Brown MR, Chico RM, Bretscher MT, Drakeley C, Jensen HT. Will More of the Same Achieve Malaria Elimination? Results from an Integrated Macroeconomic Epidemiological Demographic Model. *Am J Trop Med Hyg*. 2020 Nov; 103 (5):1871–82.

2. WHO. Word Malaria Report 2021. Word Malaria report Geneva: World Health Organization. (2021). Licence: CC. 2021. 2013–2015 p.

3. Mishra KP, Ganju L, Sairam M, Banerjee PK, Sawhney RC. A review of high throughput technology for the screening of natural products. Biomed Pharmacother [Internet]. 2008 cited 2008; 62 (2):94–8. Available from: https://www.sciencedirect.com/science/article/pii/S0753 332207001278

4. Tanrikulu Y, Krüger B, Proschak E. The holistic integration of virtual screening in drug discovery. *Drug Discov Today*. 2013 Apr; 18 (7–8):358–64.

5. Nyamai DW, Tastan Bishop Ö. Identification of Selective Novel Hits against Plasmodium falciparum Prolyl tRNA Synthetase Active Site and a Predicted Allosteric Site Using in silico Approaches. *Int J Mol Sci*. 2020 May; 21 (11).

6. Shah P, Tiwari S, Siddiqi MI. Recent progress in the identification and development of anti-malarial agents using virtual screening based approaches. *Comb Chem High Throughput Screen*. 2015; 18 (3):257–68.

7. Ripphausen P, Nisius B, Bajorath J. State-of-the-art in ligand-based virtual screening. *Drug Discov Today*. 2011 May; 16 (9–10):372–6.

8. Varela-Rial A, Majewski M, De Fabritiis G. Structure based virtual screening: Fast and slow. WIREs Comput Mol Sci [Internet]. 2022 Mar 1 cited 2022; 12 (2):e1544. Available from: https://doi.org/10.1002/wcms.1544

9. Widyananda MH, Kurniasari CA, Alam FM, Rizky WC, Dings TGA, Ansori ANM, et al. Exploration of Potentially Bioactive Compounds from Fingerroot (Boesenbergia rotunda L.) as Inhibitor of Atherosclerosis-Related Proteins (CETP, ACAT1, OSC, sPLA2): An in silico Study. *Jordan J Pharm Sci*. 2023; 16 (3):550–64.

10. Babandi A, Anosike CA, Ezeanyika LUS, Yelekçi K, Uba AI. Molecular modeling studies of some phytoligands from Ficus sycomorus fraction as potential inhibitors of cytochrome CYP6P3 enzyme of Anopheles coluzzii. *Jordan J Pharm Sci*. 2022; 15 (2):258–75.

11. Ghislat G, Rahman T, Ballester PJ. Recent progress on the prospective application of machine learning to structure-based virtual screening. *Curr Opin Chem Biol*. 2021 Dec; 65:28–34.

12. Kimber TB, Chen Y, Volkamer A. Deep Learning in Virtual Screening: Recent Applications and Developments. *Int J Mol Sci*. 2021 Apr; 22 (9).

13. Ibba M, Soll D. Aminoacyl-tRNA synthesis. *Annu Rev Biochem*. 2000; 69:617–50.

14. Manickam Y, Chaturvedi R, Babbar P, Malhotra N, Jain V, Sharma A. Drug targeting of one or more aminoacyl-tRNA synthetase in the malaria parasite Plasmodium falciparum. *Drug Discov Today*. 2018 Jun; 23 (6):1233–40.

15. Keller TL, Zocco D, Sundrud MS, Hendrick M, Edenius M, Yum J, et al. Halofuginone and other febrifugine derivatives inhibit prolyl-tRNA synthetase. *Nat Chem Biol*. 2012 Feb; 8 (3):311–7.

16. Herman JD, Pepper LR, Cortese JF, Estiu G, Galinsky K, Zuzarte-Luis V, et al. The cytoplasmic prolyl-tRNA synthetase of the malaria parasite is a dual-stage target of febrifugine and its analogs. *Sci Transl Med*. 2015 May; 7 (288):288ra77.

17. Jain V, Yogavel M, Kikuchi H, Oshima Y, Hariguchi N, Matsumoto M, et al. Targeting Prolyl-tRNA Synthetase to Accelerate Drug Discovery against Malaria, Leishmaniasis, Toxoplasmosis, Cryptosporidiosis, and Coccidiosis. *Structure*. 2017 Oct; 25 (10):1495-1505.e6.

18. Jain V, Yogavel M, Oshima Y, Kikuchi H, Touquet B, Hakimi MA, et al. Structure of Prolyl-tRNA Synthetase-Halofuginone Complex Provides Basis for Development of Drugs against Malaria and Toxoplasmosis. *Structure*. 2015 May; 23 (5):819–29.

19. Son J, Lee EH, Park M, Kim JH, Kim J, Kim S, et al. Conformational changes in human prolyl-tRNA synthetase upon binding of the substrates proline and ATP and the inhibitor halofuginone. *Acta Crystallogr D Biol Crystallogr*. 2013 Oct; 69 (Pt 10):2136–45.

20. Hewitt SN, Dranow DM, Horst BG, Abendroth JA, Forte B, Hallyburton I, et al. Biochemical and Structural Characterization of Selective Allosteric Inhibitors of the Plasmodium falciparum Drug Target, Prolyl-tRNA-synthetase. *ACS Infect Dis*. 2017 Jan; 3 (1):34–44.

21. Nyamai DW, Tastan Bishop Ö. Identification of Selective Novel Hits against Plasmodium falciparum Prolyl tRNA Synthetase Active Site and a Predicted Allosteric Site Using in silico Approaches. *Int J Mol Sci*. 2020 May; 21 (11).

22. Sterling T, Irwin JJ. ZINC 15 – Ligand Discovery for Everyone. *J Chem Inf Model* [Internet]. 2015 Nov 23 cited 2015; 55 (11):2324–37. Available from: https://doi.org/10.1021/acs.jcim.5b00559

23. Sunseri J, Koes DR. Pharmit: interactive exploration of chemical space. *Nucleic Acids Res*. 2016 Jul; 44 (W1):W442-8.

24. Lipinski CA, Lombardo F, Dominy BW, Feeney PJ. Experimental and computational approaches to estimate solubility and permeability in drug discovery and development settings. Adv Drug Deliv Rev [Internet]. 1997 cited 1997; 23 (1):3–25. Available from: https://www.sciencedirect.com/science/article/pii/S0169409X96004231

25. Lagorce D, Bouslama L, Becot J, Miteva MA, Villoutreix BO. FAF-Drugs4: free ADME-tox filtering computations for chemical biology and early stages drug discovery. *Bioinformatics*. 2017 Nov; 33 (22):3658–60.

26. Baell JB, Holloway GA. New Substructure Filters for Removal of Pan Assay Interference Compounds (PAINS) from Screening Libraries and for Their Exclusion in Bioassays. *J Med Chem* [Internet]. 2010 Apr 8 cited 2010; 53 (7):2719–40. Available from: https://doi.org/10.1021/jm901137j

27. Maier JA, Martinez C, Kasavajhala K, Wickstrom L, Hauser KE, Simmerling C. ff14SB: Improving the Accuracy of Protein Side Chain and Backbone Parameters from ff99SB. *J Chem Theory Comput* [Internet]. 2015 Aug 11 cited 2015; 11 (8):3696–713. Available from: https://doi.org/10.1021/acs.jctc.5b00255

28. Gasteiger J, Marsili M. Iterative partial equalization of orbital electronegativity—a rapid access to atomic charges. Tetrahedron [Internet]. 1980 cited 1980; 36 (22):3219–28. Available from: https://www.sciencedirect.com/science/article/pii/0040402080801682

29. Pettersen EF, Goddard TD, Huang CC, Couch GS, Greenblatt DM, Meng EC, et al. UCSF Chimera--a visualization system for exploratory research and analysis. *J Comput Chem*. 2004 Oct; 25 (13):1605–12.

30. Raček T, Schindler O, Toušek D, Horský V, Berka K, Koča J, et al. Atomic Charge Calculator II: web-based tool for the calculation of partial atomic charges. *Nucleic Acids Res* [Internet]. 2020 Jul 2 cited 2020; 48 (W1):W591–6. Available from: https://doi.org/10.1093/nar/gkaa367

31. Kramer B, Rarey M, Lengauer T. Evaluation of the FLEXX incremental construction algorithm for protein-ligand docking. *Proteins*. 1999 Nov; 37 (2):228–41.

32. Triballeau N, Acher F, Brabet I, Pin JP, Bertrand HO. Virtual screening workflow development guided by the "receiver operating characteristic" curve approach. Application to high-throughput docking on metabotropic glutamate receptor subtype 4. *J Med Chem*. 2005 Apr; 48 (7):2534–47.

33. Truchon JF, Bayly CI. Evaluating Virtual Screening Methods: Good and Bad Metrics for the "Early Recognition" Problem. *J Chem Inf Model* [Internet]. 2007 Mar 1 cited 2007; 47 (2):488–508. Available from: https://doi.org/10.1021/ci600426e

34. Bura E, Gastwirth JL. The Binary Regression Quantile Plot: Assessing the Importance of Predictors in Binary Regression Visually. *Biometrical J* [Internet]. 2001 Feb 1 cited 2001; 43 (1):5–21. Available from: https://doi.org/10.1002/1521-4036(200102)43:1%3C5::AID-BIMJ5%3E3.0.CO

35. Empereur-Mot C, Zagury JF, Montes M. Screening Explorer–An Interactive Tool for the Analysis of Screening Results. *J Chem Inf Model* [Internet]. 2016 Dec 27 cited 2016; 56 (12):2281–6. Available from: https://doi.org/10.1021/acs.jcim.6b00283

36. Abraham MJ, Murtola T, Schulz R, Páll S, Smith JC, Hess B, et al. GROMACS: High performance molecular simulations through multi-level parallelism from laptops to supercomputers. *SoftwareX* [Internet]. 2015 cited 2015; 1–2:19–25. Available from: https://www.sciencedirect.com/science/article/pii/S2352711015000059

37. Jorgensen WL, Chandrasekhar J, Madura JD, Impey RW, Klein ML. Comparison of simple potential functions for simulating liquid water. \jcp. 1983 Jul; 79 (2):926–35.

38. Izadi S, Aguilar B, Onufriev A V. Protein–Ligand Electrostatic Binding Free Energies from Explicit and Implicit Solvation. *J Chem Theory Comput* [Internet]. 2015 Sep 8 cited 2015; 11 (9):4450–9. Available from: https://doi.org/10.1021/acs.jctc.5b00483

39. Essmann U, Perera L, Berkowitz ML, Darden T, Lee H, Pedersen LG. A smooth particle mesh Ewald method. *J Chem Phys* [Internet]. 1995 Nov 15 cited 1995; 103 (19):8577–93. Available from: https://doi.org/10.1063/1.470117

40. Bussi G, Donadio D, Parrinello M. Canonical sampling through velocity rescaling. *J Chem Phys* [Internet]. 2007 Jan 3 cited 2007; 126 (1):14101. Available from: https://doi.org/10.1063/1.2408420

41. Parrinello M, Rahman A. Polymorphic transitions in single crystals: A new molecular dynamics method. *J Appl Phys* [Internet]. 1981 Dec 1 cited 1981; 52 (12):7182–90. Available from: https://doi.org/10.1063/1.328693

42. 42. Kumari R, Kumar R, Lynn A. g_mmpbsa—A GROMACS Tool for High-Throughput MM-PBSA Calculations. *J Chem Inf Model* [Internet]. 2014 Jul 28 cited 2014; 54 (7):1951–62. Available from: https://doi.org/10.1021/ci500020m

43. Trager W, Jensen JB. Human malaria parasites in continuous culture. Science. 1976 Aug; 193 (4254):673–5.

44. Khasanah U, WidyaWaruyanti A, Hafid AF, Tanjung M. Antiplasmodial Activity of Isolated Polyphenols from Alectryon serratus Leaves Against 3D7 Plasmodium falciparum. *Pharmacognosy Res*. 2017 Dec; 9 (Suppl 1):S57–60.

45. Kumar A, Zhang KYJ. Hierarchical virtual screening approaches in small molecule drug discovery. *Methods*. 2015 Jan; 71:26–37.

46. Réau M, Langenfeld F, Zagury JF, Lagarde N, Montes M. Decoys Selection in Benchmarking Datasets: Overview and Perspectives [Internet]. Vol. 9, *Frontiers in Pharmacology*. 2018 cited 2018; Available from: https://www.frontiersin.org/articles/10.3389/fphar.2018.00011

47. 47. Xing J, Li Q, Zhang S, Liu H, Zhao L, Cheng H, et al. Identification of dipeptidyl peptidase IV inhibitors: virtual screening, synthesis and biological evaluation. *Chem Biol Drug Des*. 2014 Sep; 84 (3):364–77.

48. Al-Sha'er MA, Basheer HA, Taha MO. Discovery of new PKN2 inhibitory chemotypes via QSAR-guided selection of docking-based pharmacophores. *Mol Divers*. 2023 Feb; 27 (1):443–62.

49. Fawcett T. An introduction to ROC analysis. *Pattern Recognit Lett*. 2006; 27 (8):861–74.

50. Empereur-Mot C, Guillemain H, Latouche A, Zagury JF, Viallon V, Montes M. Predictiveness curves in virtual screening [Internet]. Vol. 7, *Journal of cheminformatics. Laboratoire Génomique Bioinformatique et Applications*, EA 4627, Conservatoire National des Arts et Métiers, 292 rue Saint Martin, 75003 Paris, France.; 2015 cited 2015; p. 52. Available from: http://europepmc.org/abstract/MED/26539250

51. Thomsen R, Christensen MH. MolDock: A New Technique for High-Accuracy Molecular Docking. *J Med Chem* [Internet]. 2006 Jun 1 cited 2006; 49 (11):3315–21. Available from: https://doi.org/10.1021/jm051197e

52. Feher M. Consensus scoring for protein-ligand interactions. *Drug Discov Today*. 2006 May; 11 (9–10):421–8.

53. Humphrey W, Dalke A, Schulten K. VMD: Visual molecular dynamics. *J Mol Graph* [Internet]. 1996 cited 1996; 14 (1):33–8. Available from: https://www.sciencedirect.com/science/article/pii/0263785596000185

54. Genheden S, Ryde U. The MM/PBSA and MM/GBSA methods to estimate ligand-binding affinities. *Expert Opin Drug Discov*. 2015 May; 10 (5):449–61.

55. Poli G, Granchi C, Rizzolio F, Tuccinardi T. Application of MM-PBSA Methods in Virtual Screening. *Molecules*. 2020 Apr; 25 (8).

56. King E, Aitchison E, Li H, Luo R. Recent Developments in Free Energy Calculations for Drug Discovery [Internet]. Vol. 8, *Frontiers in Molecular Biosciences*. 2021 cited 2021; Available from: https://www.frontiersin.org/articles/10.3389/fmolb.2021.712085

57. Bhatt TK, Kapil C, Khan S, Jairajpuri MA, Sharma V, Santoni D, et al. A genomic glimpse of aminoacyl-tRNA synthetases in malaria parasite Plasmodium falciparum. *BMC Genomics* [Internet]. 2009 cited 2009; 10 (1):644. Available from: https://doi.org/10.1186/1471-2164-10-644

اكتشاف مثبط إستروزي لأنزيم برويل-تي آر إن إيه المحتمل عبر الفحص الافتراضي والتجربة في المختبر ضد البلاسموديوم فالسيباروم

تيغار أحسندو يونيارتا [1]* ، إي غيدي أري سومارتا [1]، توفيق محمد فقيه [2]، راسيتا هانداياني [3]، دوي سياه فيترا رمضان [4]

[1]قسم الكيمياء الصيدلانية، كلية الصيدلة، جامعة سورابايا، سورابايا، إندونيسيا

[2]قسم الصيدلة، كلية الرياضيات والعلوم الطبيعية، جامعة باندونج الإسلامية، باندونج، إندونيسيا

[3]قسم العلوم الصيدلانية، كلية الصيدلة، جامعة أيرلانجا، سورابايا، إندونيسيا

[4]قسم الصيدلة، المعهد الصحي لوزارة الصحة، ماكاسار، إندونيسيا

ملخص

الأهداف: هدفت هذه الدراسة إلى تحديد مركبات مضادة للملاريا الجديدة بناءً على مثبطات موقع مختلف للبروليل-تي-آر-إيه سينثيتيز باستخدام الفرز الافتراضي التسلسلي الهرمي.

المواد والطرق: تم تصميم نموذج الفارماكوفور في البداية، بناءً على بيانات العلاقة بين البنية والنشاط بين عدة مثيلات للبيرازول-اليوريا وقيمتها الإنزيمية IC50. تم تطبيق النموذج المحصل عليه على قاعدة بيانات ZINC15، تليها عملية فلترة المرشحات المتعلقة بشبهات العقاقير والتسمم و PAINS. تم تثبيت المركبات المصنفة باستخدام طريقة التثبيت المصادق عليها ضد إنزيم بروليل-تي-آر-إيه سينثيتيز لـ P. falciparum. تم ترتيب مواضع التثبيت الناتجة بناءً على درجة التثبيت وإعادة التقييم بناءً على معايير الفارماكوفور. تم الحصول على أفضل خمسة مركبات من هذه الخطوة ومن ثم تم تقييمها باستخدام المحاكاة الديناميكية الجزيئية للتحقق من ثباتها وديناميات الروابط الهيدروجينية لأكثر من 50 نانوثانية. تم أيضًا إجراء تحليل MM-PBSA لتقدير طاقة الربط الحرة للمركبات. وأخيرًا، تم التحقق من النشاط الحيوي للمركبات كمرشحات مضادة للملاريا ضد السلالة D7.3

النتائج: أظهرت النتائج أن جميع المركبات الخمس المحصل عليها من الفرز الافتراضي تمتلك فعالية ميكرومولارية وكان من in vitro.

الكلمات الدالة: مضاد للملاريا، ديناميكا جزيئية، بلاسموديوم فالسيباروم، بروليل-تي-آر-إيه سينثيتيز، فرز افتراضي.